Cell. Mol. Life Sci. (2016) 73:2583–2599
DOI 10.1007/s00018-016-2132-2

Cellular and Molecular Life Sciences

ORIGINAL ARTICLE

Fast skeletal myofibers of *mdx* mouse, model of Duchenne muscular dystrophy, express connexin hemichannels that lead to apoptosis

Luis A. Cea[1,2] · Carlos Puebla[2,3] · Bruno A. Cisterna[2,3] · Rosalba Escamilla[2,3] · Aníbal A. Vargas[2] · Marina Frank[4] · Paloma Martínez-Montero[5] · Carmen Prior[5] · Jesús Molano[5] · Isabel Esteban-Rodríguez[6] · Ignacio Pascual[7] · Pía Gallano[8] · Gustavo Lorenzo[9] · Héctor Pian[10] · Luis C. Barrio[11] · Klaus Willecke[4] · Juan C. Sáez[2,3]

Received: 18 August 2015 / Revised: 15 December 2015 / Accepted: 7 January 2016 / Published online: 23 January 2016

Abstract Skeletal muscles of patients with Duchenne muscular dystrophy (DMD) show numerous alterations including inflammation, apoptosis, and necrosis of myofibers. However, the molecular mechanism that explains these changes remains largely unknown. Here, the involvement of hemichannels formed by connexins (Cx HCs) was evaluated in skeletal muscle of *mdx* mouse model of DMD. Fast myofibers of *mdx* mice were found to express three connexins (39, 43 and 45) and high sarcolemma permeability, which was absent in myofibers of *mdx* $Cx43^{fl/fl}Cx45^{fl/fl}$:Myo-Cre mice (deficient in skeletal muscle Cx43/Cx45 expression). These myofibers did not show elevated basal intracellular free Ca^{2+} levels, immunoreactivity to phosphorylated p65 (active NF-κB), eNOS and annexin V/active Caspase 3 (marker of apoptosis) but presented dystrophin immunoreactivity. Moreover, muscles of *mdx* $Cx43^{fl/fl}Cx45^{fl/fl}$:Myo-Cre mice exhibited partial decrease of necrotic features (big cells and high creatine kinase levels). Accordingly, these muscles showed similar macrophage infiltration as control *mdx* muscles. Nonetheless, the hanging test performance of *mdx* $Cx43^{fl/fl}Cx45^{fl/fl}$:Myo-Cre mice was significantly better than that of control *mdx* $Cx43^{fl/fl}$-$Cx45^{fl/fl}$ mice. All three Cxs found in skeletal muscles of *mdx* mice were also detected in fast myofibers of biopsy specimens from patients with muscular dystrophy. Thus, reduction of Cx expression and/or function of Cx HCs may be potential therapeutic approaches to abrogate myofiber apoptosis in DMD.

Keywords Connexons · Evans blue uptake · $P2X_7$ receptors · Pannexin1 · NF-κB · Cell death

✉ Luis A. Cea
luiscea@med.uchile.cl

✉ Juan C. Sáez
jsaez@bio.puc.cl

[1] Present Address: Present: Program of Anatomy and Developmental Biology, Institute of Biomedical Sciences, Faculty of Medicine, University of Chile, Santiago, Chile

[2] Departamento de Fisiología, Pontificia Universidad Católica de Chile, Av. Libertador Bernardo O'Higgins 340, Santiago, Chile

[3] Centro Interdisciplinario de Neurociencias de Valparaíso, Valparaíso, Chile

[4] Division of Molecular Genetics, Life and Medical Sciences Institute, University of Bonn, 53115 Bonn, Germany

[5] Unidad de Genética Molecular-INGEMM, Hospital Universitario La Paz-IdIPAZ, Madrid, Spain

[6] Servicio de Anatomía Patológica, Hospital Universitario La Paz-IdIPAZ, Madrid, Spain

[7] Servicio de Neuropediatría, Hospital Universitario La Paz-IdIPAZ, Madrid, Spain

[8] Servicio de Genética, Hospital Santa Creu i Sant Pablo-CIBERER, Barcelona, Spain

[9] Servicio de Pediatria, "Ramón y Cajal" Hospital-IRYCIS, Madrid, Spain

[10] Servicio de Anatomía Patológica, "Ramón y Cajal" Hospital-IRYCIS, Madrid, Spain

[11] Unidad de Neurología Experimental, "Ramón y Cajal" Hospital-IRYCIS, Madrid, Spain

Introduction

Duchenne muscular dystrophy (DMD, MIM#30037), the most frequent human muscular genetic disease, affects 1 of 3500 males born [1]. DMD is caused by mutation in dystrophin (427 kDa; Xp21.2-p21.1), which links the cytoskeleton to the molecular aggregate termed dystroglycan complex [2]. This complex is present on the surface of the sarcolemma where it interacts with the extracellular matrix. The condition is currently being detected at an early age but survival has not changed significantly since there are no effective treatments for this disease [3].

Since the *mdx* mouse shares several characteristics with the human muscular dystrophy illness, it is frequently used to further knowledge on this disease [4]. In these animals, the absence of dystrophin in myofibers is associated with an early increase in intracellular free Ca^{2+} [5] and Na^{+} [6] levels. In addition, membrane permeability to dyes such as procion orange (FW 631 g mol^{-1}) and Evans blue (EB^{4-}, FW 960.82 g mol^{-1}) also increases and has been interpreted as skeletal muscle damage in vivo [7, 8]. Nonetheless, this finding might need reinterpretation since the sarcolemma of denervated myofibers shows similar changes including permeability to EB^{4-} and has been shown to result from permeabilization of the sarcolemma by connexin (Cx) hemichannels [9].

Hemichannels are non-selective cationic channels permeable to ions (e.g. Ca^{2+} and Na^{+}) and small compounds, including signaling molecules such as ATP and NAD^{+} and dyes including ethidium (Etd^{+}) and EB^{4-} [9, 10]. Ionic gadolinium (Gd^{3+}), a connexin hemichannel (Cx HC) blocker [11], has been used to prevent muscular damage in *mdx* mice [6] and to block stretch-activated sarcolemma channels reducing Ca^{2+} influx in *mdx* mice myofibers [12]. However, the molecular identity of these channels remains unknown and a putative identity could be Cx HCs since they are mechanosensitive [13], permeable to Ca^{2+} [14, 15] and blocked by lanthanides including Gd^{3+} and La^{3+} [9]. Moreover, TRPV2 channels have been proposed to be a relevant membrane pathway through which Ca^{2+} influx increases and consequently intracellular free Ca^{2+} levels increases in myofibers of *mdx* mice [16]. Accordingly, a dominant-negative TRPV2 channel in skeletal myofibers renders the sarcolemma of dystrophic myofibers less permeable to Ca^{2+} and improves muscle performance [16]. Muscles of *mdx* mice also show upregulation of pannexin1 (Panx1) channels [17] and purinergic ionotropic $P2X_7$ receptors ($P2X_7Rs$) [18, 19]. The possible relevance of at least of Panx1 channels in the muscle pathogenesis has been ruled out [19]. However, it remains unknown whether skeletal muscles of *mdx* mice express Cx HCs, of which at least Cx43 HCs have been shown to be permeable to Na^{+} and Ca^{2+} [15, 20].

In the present study, we observed the presence of Cxs 39, 43 and 45 in dystrophic mouse *mdx* skeletal muscle. These proteins were found to form functional hemichannels in myofibers of *mdx* mice, which are absent in normal fibers. We also observed that $P2X_7Rs$ and Panx1 channels participate in controlling the sarcolemma permeability of dystrophic myofibers and apoptosis was not detected in myofibers deficient in Cx43/Cx45 expression. However, the latter still show significant necrotic cell death. Since Cxs 40.1, 43 and 45 were also detected in biopsy specimen of DMD patients but not in those of health individuals, it is suggested that de novo expression of functional Cx HCs plays a similar role in the pathogenesis of DMD.

Results

Skeletal myofibers of *mdx* mice express connexins 39, 43 and 45 and show enhanced hemichannel activity controlled by $P2X_7Rs$

Since sarcolemma permeability to Ca^{2+} of *mdx* myofibers is known to be high [12], we decided to evaluate the presence and distribution of proteins known to form non-selective membrane channels. To this end, we studied the presence of Cxs 39, 43 and 45, Panx1 and protein subunits $P2X_7R$ and the transient receptor potential type V2 (TRPV2) channel [21–23]. All these proteins, with the exception of Panx1, are not expressed by myofibers after innervation and throughout adulthood [24, 25]. For that we evaluated the levels of each protein aforementioned through western blot analysis in *tibialis anterior* (TA) muscle homogenates from control (C57) and *mdx* mice, detecting a significant increase in levels of all protein evaluated in *mdx* muscle, which did not occur in *mdx* muscles deficient in Cx43/Cx45 expression (*mdx* M-C) (Fig. 1). However, levels of Cx43 and Cx45 in control and *mdx* M-C muscles were comparable probably due to the contamination with other cell types present in tissue homogenates, including vascular and satellite cells that express pannexin1 and connexins [26, 27]. The absence of Cx43 and Cx45 did not affect the increase in Cx39 levels and only partially prevented the increase in $P2X_7Rs$, but levels of Cx43, Cx45, Panx1 and TRPV2 channels were as in control muscles (Fig. 1). Then, the presence of these proteins specifically in myofibers was evaluated by immunofluorescence analysis of TA muscle cross sections. Accordingly, myofibers of TA muscles of control mice only presented Panx1 reactivity (Fig. 2). However, the sarcolemma of *mdx* myofibers showed high reactivity for all three Cxs studied as well as for $P2X_7R$ and TRPV2 channel (Fig. 2). The reactivity of Panx1 in *mdx* muscles

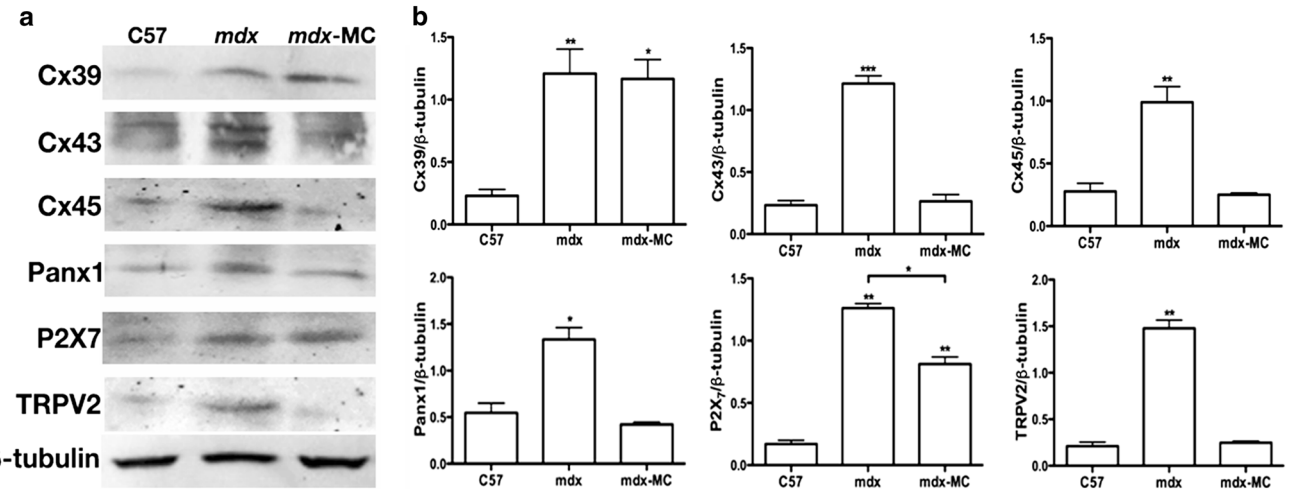

Fig. 1 Levels of Cx39, Cx43, Cx45, Panx1, $P2X_7R$ are increased in skeletal muscles of *mdx* mice. *Tibialis anterior* (TA) muscles were extracted from control (C57), *mdx* and *mdx* with myofibers deficient in Cx43 and Cx45 expression mice (*mdx* M-C). Then, muscle tissue was homogenized and processed for western blot analysis. The relative levels of Cx39, Cx43, Cx45, Panx1, $P2X_7R$ and TRPV2 channels were analyzed. Relative β-Tubulin levels were measured as sample loading control. **a** Representative blot. **b** Quantification of three independent experiments as shown in **a**

was notably higher than in muscles of control animals (Fig. 2). Despite the lack of Cx43/Cx45 expression TA muscles of *mdx* $Cx43^{fl/fl}Cx45^{fl/fl}$:Myo-Cre mice still presented reactivity for Cx39, Panx1 and P2X7R (Fig. 2). However, it was evident that these muscles were devoid of TRPV2 reactivity (Fig. 2). Throughout this paper, we use the designation C57 as an abbreviation for the control mouse strain C57Bl/6 that harbored the corresponding Cx but not the *mdx* mutation.

Skeletal myofibers from *mdx* mice show enhanced membrane permeability to Evans blue that is inhibited by hemichannel and P2XR blockers

Since skeletal myofibers of *mdx* mice show Evans blue (EB^{4-}) uptake in vivo [7, 8] and the sarcolemma of denervated myofibers is permeable to EB^{4-} through a pathway inhibited by blockers of poorly selective membrane channels [9], we explored whether carbenoxolone (CBX), which is a hemichannel and $P2X_7R$ inhibitor [28] and brilliant blue G (BBG) inhibitor of Panx1 channels and $P2X_7R$ [28] would affect EB^{4-} uptake in *mdx* myofibers in vivo. To this end, control and *mdx* mice were treated with 80 mg/kg CBX or 45 mg/kg BBG 20 min before EB^{4-} injection. Intense intracellular EB^{4-} staining was found in cross sections of TA muscles obtained from *mdx* mice (Fig. 3). However, muscle samples of control mice or *mdx* mice treated with CBX or BBG did not show intracellular EB^{4-} staining (Fig. 3). The possible role of membrane damage was then tested in *mdx* mice injected with Rhodamine Dextran (RD) (10 kDa), which is a molecular probe with a size above the exclusion limit of non-selective channels permeable to small molecules (between 1 and 2 kDa). RD staining was detected only in the interstitial spaces of TA muscles of these animals (Fig. 3), thus indicating the absence of cell membrane damage.

To further test if Cx HCs mediated the EB^{4-} uptake observed in TA muscles of *mdx* mice, we repeated the assay in *mdx* $Cx43^{fl/fl}Cx45^{fl/fl}$:Myo-Cre (myofibers deficient in Cx43/Cx45 expression) and *mdx* $Cx43^{fl/fl}Cx45^{fl/fl}$ mice (control mice). EB^{4-} fluorescence was clearly seen in numerous myofibers in cross sections of TA muscles of *mdx* $Cx43^{fl/fl}Cx45^{fl/fl}$ mice (Fig. 3). However, intracellular EB^{4-} staining was absent in all myofibers of TA muscles of *mdx* $Cx43^{fl/fl}Cx45^{fl/fl}$:Myo-Cre mice (Fig. 3), which is consistent with the notion that EB^{4-} crosses the sarcolemma through Cx HCs in myofibers of *mdx* animals.

The sarcolemma of isolated myofibers presents functional hemichannels

Since the above results suggest the involvement of Cx HCs increasing the sarcolemma permeability of *mdx* myofibers, we decided to further test the presence of functional hemichannels in freshly isolated myofibers. Ethidium (Etd^+) and different channel blockers were used as described previously for denervated or inflamed myofibers [9, 24].

While C57 myofibers presented only Panx1 reactivity, *mdx* myofibers were positive for Cx39, Cx43 and Cx45 in addition to Panx1 (Fig. 4a). In agreement with the content of HC forming proteins, myofibers of *mdx* mice presented

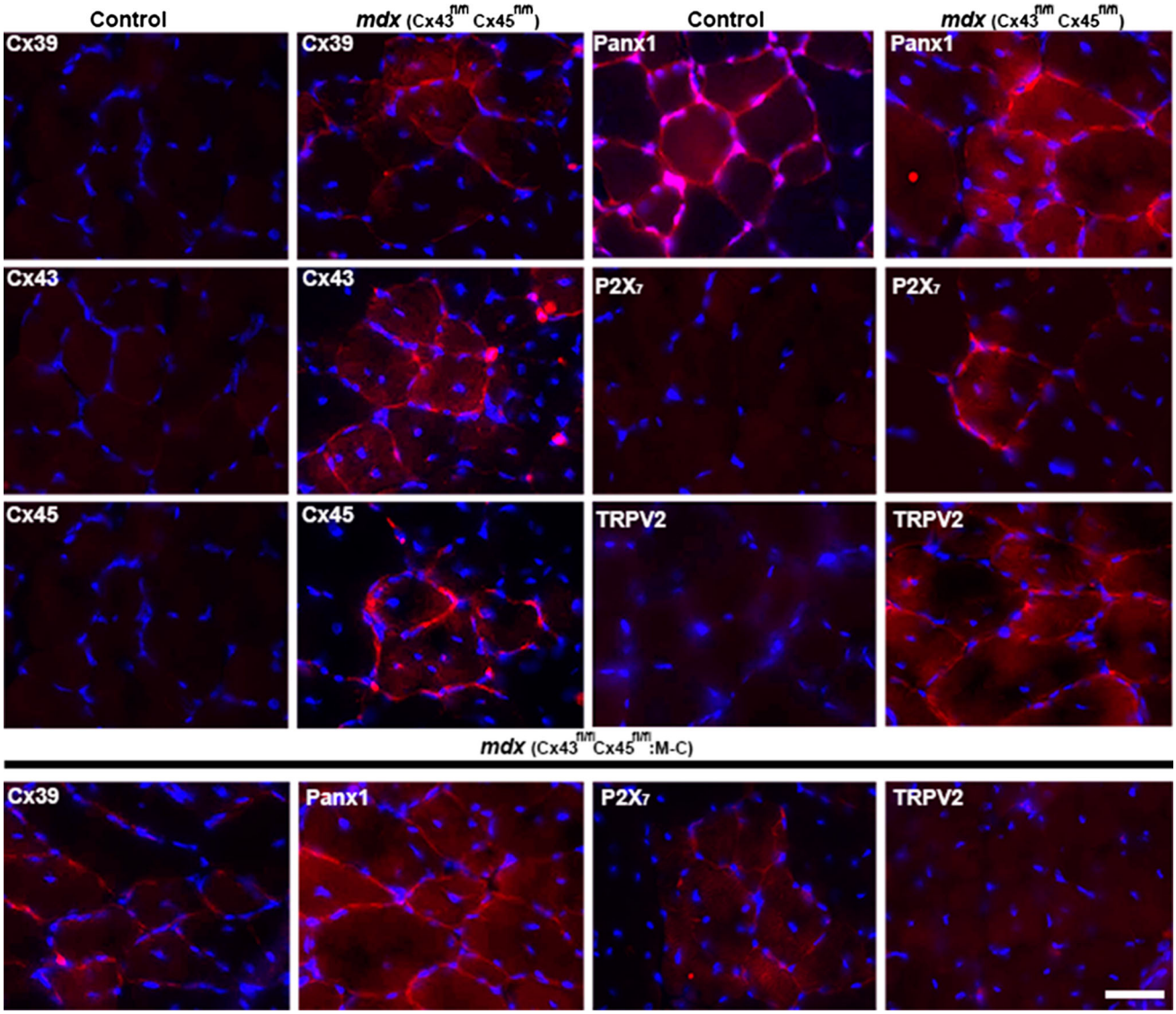

Fig. 2 The presence and distribution of Cx39, Cx43, Cx45, Panx1, $P2X_7R$ and TRPV2 channel in *tibialis anterior* muscle from C57 and *mdx* mice. *Tibialis anterior* (TA) muscles were extracted from control ($Cx43^{fl/fl}Cx45^{fl/fl}$) and *mdx* ($Cx43^{fl/fl}Cx45^{fl/fl}$) mice, and cross sections (20 µm) were obtained. Nuclei were stained with DAPI (*blue*) and antigen–antibody complexes were detected with anti-IgGs conjugated to Cy3 (*red*). Then, the presence and distribution of Cx39, Cx43, Cx45, Panx1, $P2X_7R$ and TRPV2 were analyzed by immunofluorescence. In control (C57) sections only Panx1 showed a positive signal mostly surrounded the myofibers, while in *mdx* muscles all proteins evaluated were positive and mostly in the sarcolemma (*upper panel*). Cx39, Panx1, $P2X_7R$ and TRPV2 reactivity was evaluated in cross sections of TA from *mdx* mice deficient in Cx43 and Cx45 ($Cx43^{fl/fl}Cx45^{fl/fl}$:Myo-Cre) (*bottom panel*). *Scale bar* 50 µm (4 mice and 6 sections analyzed of each animal)

higher Etd^+ uptake (~2.3-fold) than myofibers of control animals (Fig. 4b, d). In both cases, the Etd^+ uptake rate was inhibited by 200 µM La^{3+} (~70 %) (Fig. 4d), which is a blocker of Cx HCs and P2XRs [10, 29]. The Etd^+ uptake was also drastically reduced by ^{10}Panx1 peptide, suggesting the involvement of Panx1 channels (Fig. 4d).

To unravel the role of different non-selective channels in the mechanism that could underlie the Etd^+ uptake difference between control and *mdx* myofibers, cells were acutely treated (5 min) with oxidized ATP (oATP), which blocks several P2XRs, or A740003, a selective $P2X_7R$ blocker [30]. Etd^+ uptake was drastically inhibited by oATP and A740003 in *mdx* myofibers (~80 and ~90 %, respectively), but in normal myofibers these compounds were without effect (Fig. 4c, d), and the lack of Cx43/Cx45 expression in *mdx* myofibers (*mdx*:M-C) totally prevented the increase in Etd^+ uptake, confirming the results obtained with hemichannel inhibitors (Fig. 4d).

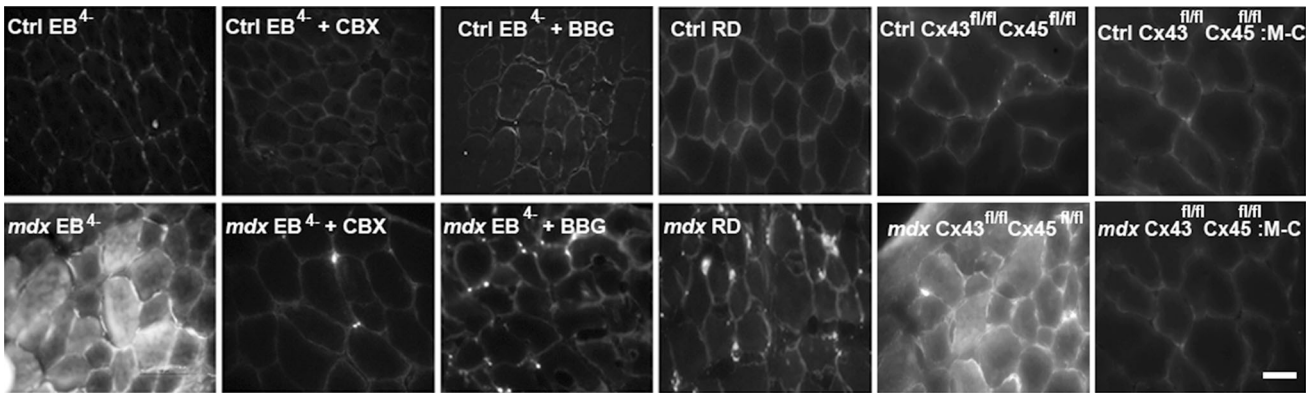

Fig. 3 Skeletal myofibers from *mdx* mice show enhanced Evans blue staining inhibited by HC and P2XR blockers. Control (Ctrl) C57, Ctrl $Cx43^{fl/fl}$ $Cx45^{fl/fl}$, Ctrl $Cx43^{fl/fl}$ $Cx45^{fl/fl}$:Myo-Cre (M-C), *mdx*, *mdx* $Cx43^{fl/fl}Cx45^{fl/fl}$ and *mdx* $Cx43^{fl/fl}$ $Cx45^{fl/fl}$:Myo-Cre (M-C) mice were injected with Evans blue (65 mg/kg EB^{4-}), and only mice that can express Cxs (Ctrl and *mdx*) were evaluated in the absence or presence of carbenoxolone (CBX, 80 mg/kg), which is a connexin hemichannel and pannexin1 channel inhibitor, brilliant blue G (BBG, 45 mg/kg), a $P2X_7R$ and Panx1 channels inhibitor or Rhodamine Dextran (RD). They were euthanized after 6 h. Then, *tibialis anterior* muscles were dissected and cross sections were obtained, mounted and excited at $\lambda = 530$ nm, and fluorescent emission was photographed at $\lambda = 595$ nm (20 µm) ($n = 4$). *Scale bar* 50 µm (4 mice and 6 sections were analyzed from each animal)

We next decided to evaluate the intracellular free Ca^{2+} signal in myofibers, because previous works have shown that these channels are permeable to Ca^{2+} [15] and that *mdx* myofibers show discrete elevated basal intracellular free Ca^{2+} levels [31]. Thus, in concordance with the elevated hemichannels activity found in *mdx* myofibers, we also detected an elevated basal intracellular free Ca^{2+} signal in these myofibers compared with control (C57) myofibers (Fig. 5), which was not detected in myofibers deficient in Cx43 and Cx45 expression (*mdx*:M-C myofibers) (Fig. 5).

The absence of Cx43 and Cx45 abrogates NF-κB activation and iNOS expression in *mdx* myofibers

Since the absence of Cx HCs abrogates the denervation-induced activation of nuclear factor kappa-light-chain-enhancer in activated B cells (NF-κB) [9], the presence and distribution of activated [phosphorylated p65 subunit (P-p65)] NF-κB was analyzed in *mdx* $Cx43^{fl/fl}Cx45^{fl/fl}$:Myo-Cre mice. While numerous myofibers of control *mdx* $Cx43^{fl/fl}Cx45^{fl/fl}$ mice showed P-p65 reactivity in the cytoplasm and nuclei (Fig. 6a), myofibers of *mdx* $Cx43^{fl/fl}Cx45^{fl/fl}$:Myo-Cre mice did not show P-p65 reactivity, indicating that NF-κB was not activated in the absence of Cx43/Cx45 expression (Fig. 6a).

Since *mdx* myofibers are known to express iNOS and generate more nitric oxide than control myofibers [32, 33], we tested if Cxs detected in *mdx* mice are related to the expression of iNOS. iNOS reactivity was mainly located in the periphery of myofibers in TA muscles of *mdx* $Cx43^{fl/fl}Cx45^{fl/fl}$ mice whereas it was absent in TA muscles of *mdx* $Cx43^{fl/fl}Cx45^{fl/fl}$:Myo-Cre mice (Fig. 6b).

Lack of Cx43/Cx45 expression completely prevents programed cell death in *mdx* skeletal muscles

Since apoptotic cells are frequent in *mdx* muscles [7, 34], we determined whether Cx expression is related to this form of cell death. To study this possibility, myofibers undergoing apoptosis were detected through the analysis of annexin V signal by using an anti-annexin V antibody [35] or by immunodetection of active caspase 3. Cross sections of TA muscles from control C57 mice did not show positive annexin V or active caspase 3 reactivity, whereas ~30 % small cells showed strong annexin V or active caspase 3 reactivity in TA muscles of *mdx* mice (Fig. 7a, b). In contrast, the absence of Cx43/Cx45 in myofibers of *mdx* mice completely prevented the appearance of the annexin V and active caspase 3 signal (Fig. 7a, b), suggesting a direct correlation between Cx43/Cx45 expression and apoptosis.

Since several *mdx* myofibers presented EB^{4-} uptake (Fig. 3) or annexin V reactivity (Fig. 7a), we evaluated whether apoptotic cells also incorporated EB^{4-}. To study this possibility, muscle sections of *mdx* mice treated with EB^{4-} were processed for annexin V detection. We found that all myofibers with intracellular EB^{4-} staining were also positive for annexin V (Fig. 7c). In contrast, myofibers deficient in Cx43/Cx45 expression did not show either EB^{4-} staining or annexin V reactivity (Fig. 7c). We then asked the following question: Are EB^{4-} stained fibers fast or slow? To answer this question, muscle sections of *mdx* mice previously injected with EB^{4-} were processed to detect myosin heavy chain type I (MHC-I), used as a marker of slow twitch fibers. We found that cells labeled with EB^{4-} were not positive for MHC-I (Fig. 7d), indicating that EB^{4-} stained fibers correspond to the fast subtype.

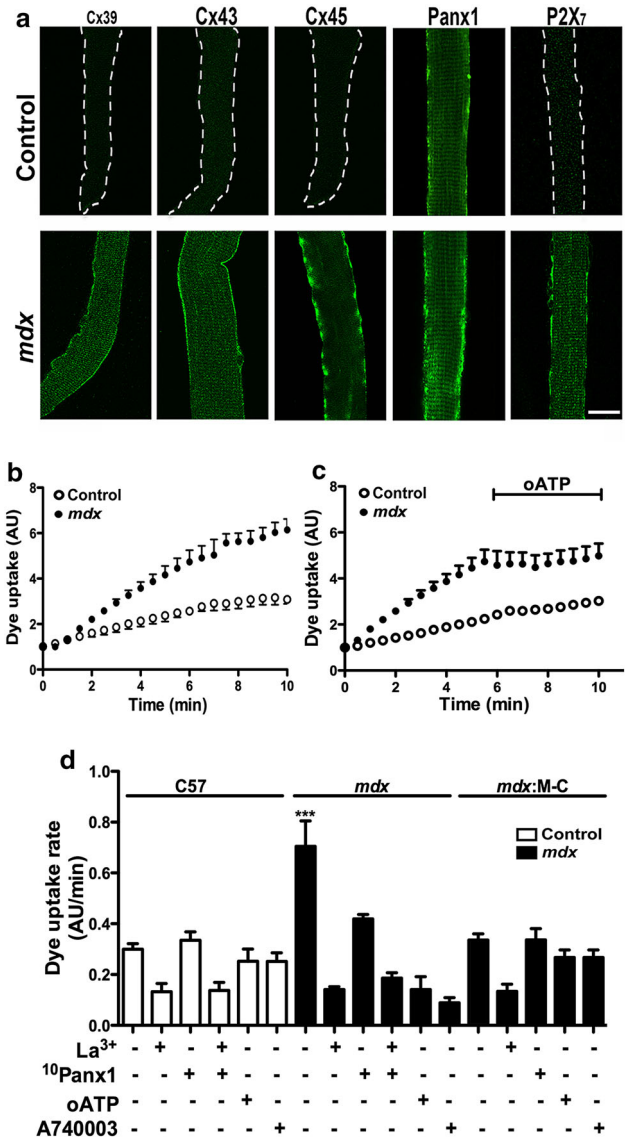

Fig. 4 Myofibers of *mdx* mice show enhanced Panx1 channels and Cx hemichannels activity controlled by $P2X_7R$. Freshly isolated myofibers from flexor digitorum brevis muscles were used for immunodetection or dye uptake assays. **a** Distribution of Cx39, Cx43, Cx45, Panx1 and $P2X_7$ (*green*) was analyzed by confocal microscopy in freshly isolated skeletal muscle fibers from control and *mdx* mice. Only Panx1 was present in control myofibers (*upper panels*, *white dash line* defines the myofiber border) but all proteins appeared in *mdx* myofibers (*bottom panel*). **b** Representative curve of ethidium (Etd^+) uptake of isolated myofibers from the same cultures as in **a**. Each value represents the fluorescence intensity over time of five myofibers (mean ± SD) under basal conditions. **c** Representative curve of Etd^+ uptake in basal conditions as in **b**, followed by the application of 100 μM oxidized ATP (oATP), a P2XR inhibitor, as indicated with a *black trace*. **d** Etd uptake rate (slopes obtained from *curves* as in **b** or **c**) after treatment with 200 μM La^{3+}, 200 μM ^{10}Panx1 peptide, 100 μM oxidized ATP (oATP) or 10 μM A740003. $^{**}P < 0.01$ ($n = 4$). *Scale bar* 20 μm

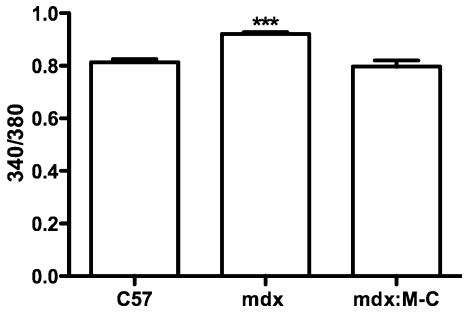

Fig. 5 The absence of Cx43/Cx45 in *mdx* skeletal myofibers prevents the elevation of basal intracellular free Ca^{2+} levels. Skeletal myofibers were isolated from C57, *mdx* and *mdx*:M-C (which do not express Cx43 and Cx45) mice and the basal intracellular Ca^{2+} signal was measured with FURA-2AM. The graph shows the 340 nm:380 nm fluorescent ratio. $^{***}P < 0.001$

The absence of Cx43/Cx45 expression partially prevents cell death by necrosis

In agreement with the occurrence of muscle regeneration promoted by cell death in skeletal muscle of *mdx* mice, the percentage of nuclei located centrally (Internal nuclei index) in cross sections of TA muscles was clearly higher in *mdx* than in C57 mice. However, TA muscles comprised of myofibers deficient in Cx43/Cx45 expression showed a significant reduction in internal nuclei index (Fig. 8). Moreover, the cross-sectional area (CSA) of myofibers analyzed in TA muscle sections stained with hematoxylin–eosin revealed that the absence of Cx43/Cx45 expression confers partial protection. We found that *mdx* TA muscles presented ~7 % myofibers with a CSA bigger than the largest one found in TA muscles of C57 mice. This was defined as a CSA value higher than 5700 μm^2 of the total number of myofibers analyzed (301 myofibers) while in control myofibers only ~0.6 % myofibers from the total number of myofibers analyzed (623 myofibers) were over 5700 μm^2, and TA muscles of *mdx* $Cx43^{fl/fl}Cx45^{fl/fl}$: Myo-Cre mice showed a significantly low number of large myofibers (~2.1 %) from the total number of myofibers analyzed (561 myofibers) (Fig. 8). In this way, we measured the total CSA because *mdx* fibers present very different size, so the average of the CSA is not a good indicator of variations in CSA, as it is shown in Fig. 8c. Then, we arbitrarily defined a threshold size for big myofibers, which was 5700 μm^2 and we estimated the percentage of total myofibers analyzed that were above this threshold size. For *mdx* myofibers it was ~7 % and for control myofibers it was only ~0.6 %. However, in *mdx* fibers deficient in Cx43/Cx45 expression it was ~2.1 %, conferring a partial protection respect to *mdx* fibers.

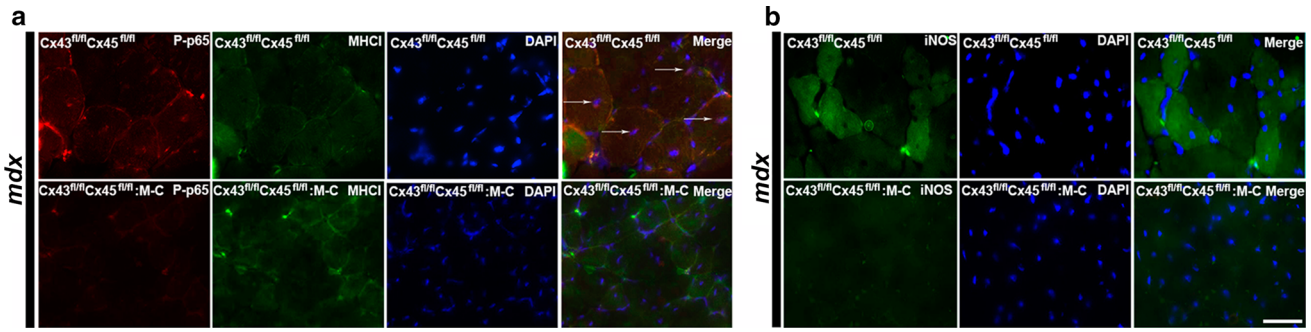

Fig. 6 The absence of Cx43/Cx45 in skeletal muscles protects from activation of NF-κB and upregulation of iNOS in *mdx* mice. Cross sections of *tibialis anterior* (TA) muscles from control $Cx43^{fl/fl}Cx45^{fl/fl}$, *mdx* $Cx43^{fl/fl}Cx45^{fl/fl}$ and *mdx* $Cx43^{fl/fl}Cx45^{fl/fl}$:Myo-Cre mice were used for immunofluorescence analysis. **a** Reactivity of phosphorylated p65 subunit of NF-κB (P-p65) (*red*). Central nuclei positive for P-p65 (*white arrow*) were detected only in *mdx* mice that express Cx43 and Cx45 (*mdx* $Cx43^{fl/fl}Cx45^{fl/fl}$). **b** iNOS reactivity (*green*) was evident in *mdx* muscles that express Cxs (*upper panels*) and absent in *mdx* muscles that cannot express Cxs (*bottom panels*). *Scale bar* 50 µm (4 mice and 6 sections were analyzed per animal)

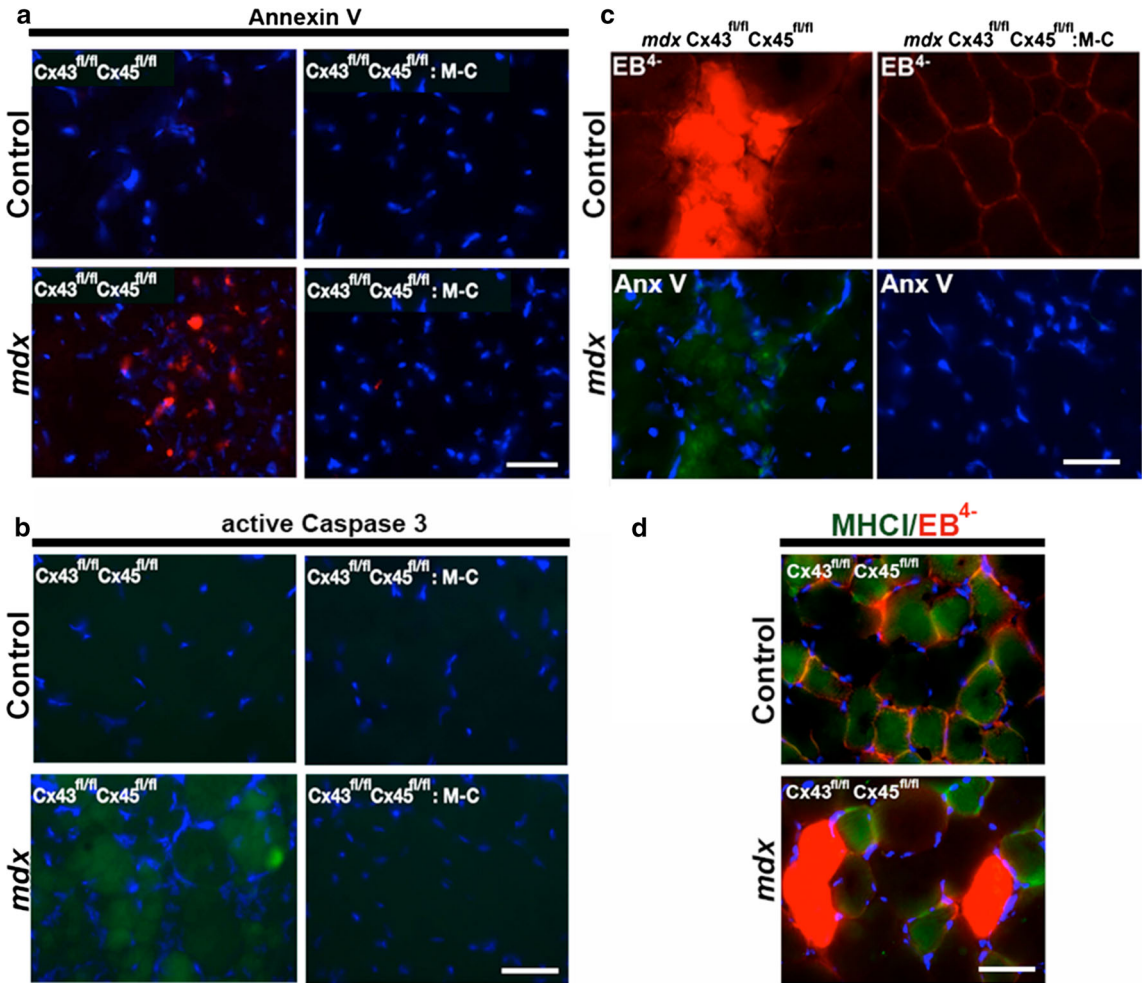

Fig. 7 The absence of Cx43/Cx45 expression drastically reduces apoptosis and dying fast myofibers are permeabilized to EB^{4-} in *mdx* mice. Cross sections of *tibialis anterior* muscles of control $Cx43^{fl/fl}$ $Cx45^{fl/fl}$, control $Cx43^{fl/fl}$ $Cx45^{fl/fl}$: Myo-Cre, *mdx* $Cx43^{fl/fl}$ $Cx45^{fl/fl}$ and *mdx* $Cx43^{fl/fl}$ $Cx45^{fl/fl}$:Myo-Cre mice were used to evaluate the reactivity of annexin V (Anx V) or Evan blue (EB^{4-}) staining. **a** Annexin V reactivity (*red*). **b** active Caspase 3 staining (green). **c** Evans blue (EB^{4-}) staining (*red*) and annexin V reactivity (*green*). **d** EB^{4-} staining (*red*) and myosin heavy chain I reactivity (MHCI positive, *green*) to denote slow myofibers. *Scale bar* 50 µm (4 mice and 6 sections were analyzed per animal)

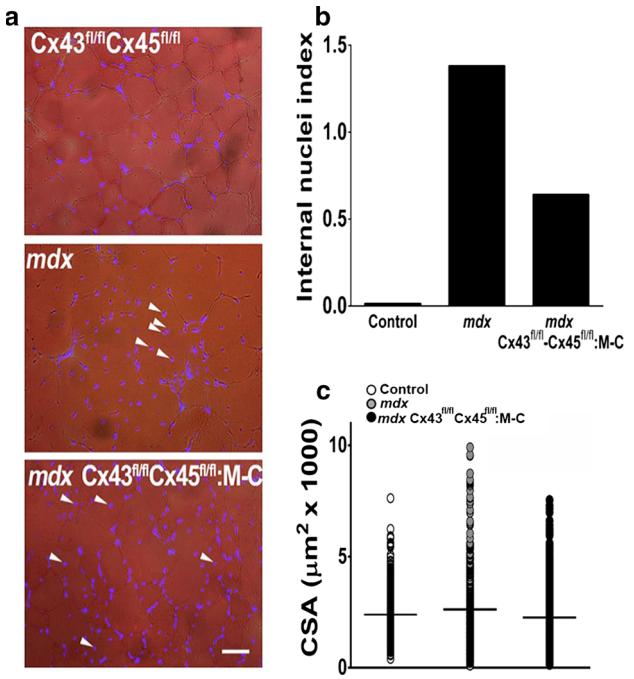

Fig. 8 *Mdx* muscles present a higher presence of big myofibers. Cross sections of *tibialis anterior* muscles obtained from Control ($Cx43^{fl/fl}$ $Cx45^{fl/fl}$, *white circles*), *mdx* (*gray circles*) and *mdx* $Cx43^{fl/fl}$ $Cx45^{fl/fl}$:Myo-Cre ($Cx43^{fl/fl}$ $Cx45^{fl/fl}$:M-C, *black circles*) mice. **a** Distribution of DAPI stained nuclei indicated in the middle panel with *white arrowheads*. *Calibration bar* 50 μm. **b** Quantification of internal nuclei index obtained from DAPI stained muscle cross sections. **c** Quantification of the cross-sectional area (CSA) in hematoxylin–eosin stained muscle cross sections. The *horizontal black line* represents the average value of CSA (4 mice and 6 sections were analyzed per animal)

In addition to apoptotic cell death, skeletal muscles of *mdx* mice and patients with DMD present necrosis reflected by high circulating levels of serum creatine kinase (CK) [36, 37]. As described previously [38], CK activity in serum samples of *mdx* mice was ~30 times higher than in serum of control animals (Fig. 9a). Moreover, the circulating CK activity of *mdx* $Cx43^{fl/fl}Cx45^{fl/fl}$:Myo-Cre mice was ~30 % lower compared to *mdx* $Cx43^{fl/fl}Cx45^{fl/fl}$ mice but remained significantly high compared to control C57 mice (Fig. 9a). This suggests that lack of Cx43/Cx45 expression confers only partial protection from necrotic cell death.

Since cell death by necrosis, but not apoptosis, retrieves inflammatory cells, and since muscles of *mdx* mice are known to present necrosis and macrophage infiltration [34, 39], we tested whether the absence of Cx43/Cx45 expression affects this phenomenon. Toward this aim, we evaluated the presence of inflammatory cells infiltrating muscular tissue through the evaluation of ED2 reactivity, which is a marker of mature macrophages [40]. As expected, *mdx* muscles presented several (30 % of myofibers presented at least 1 ED2 positive cell) ED2 positive cells, while control muscles were negative (Fig. 9b). Moreover, muscles of *mdx* $Cx43^{fl/fl}Cx45^{fl/fl}$:-Myo-Cre mice showed a similar ED2 reactivity as that of muscle of *mdx* $Cx43^{fl/fl}Cx45^{fl/fl}$ mice (Fig. 9b), suggesting that cell necrosis persists in the absence of Cx43/Cx45 expression.

The absence of Cx43/Cx45 expression in *mdx* skeletal muscles induces reappearance of dystrophin and partial muscle performance recovery

Mdx myofibers as well as human myofibers in patients with DMD show a drastic reduction or complete disappearance of dystrophin reactivity [41]. Accordingly, we found that TA muscles of 3-month-old *mdx* $Cx43^{fl/fl}Cx45^{fl/fl}$ mice showed very low dystrophin reactivity compared to muscles of control C57 mice (Fig. 10). In contrast, myofibers in *mdx* $Cx43^{fl/fl}Cx45^{fl/fl}$:Myo-Cre mice of the same age showed dystrophin reactivity with intensity and distribution comparable to that in control C57 mice (Fig. 10).

Since loss of muscle function of *mdx* mice and DMD patients is attributed to loss of functional dystrophin [42] and since we observed the reappearance of dystrophin and the absence of apoptosis in *mdx* $Cx43^{fl/fl}Cx45^{fl/fl}$:Myo-Cre mice, it was of interest to study whether the absence of Cx43/Cx45 affects muscle performance. This was evaluated by using the two or four limb "wire hanging" test. Muscle performance of 3-month-old *mdx* mice was drastically reduced in both the two and the four limb test compared to control C57 mice (Fig. 10). Muscle performance of *mdx* $Cx43^{fl/fl}Cx45^{fl/fl}$:Myo-Cre mice in both tests was significantly lower than that of control C57 mice and also significantly higher than that of *mdx* $Cx43^{fl/fl}Cx45^{fl/fl}$ mice (Fig. 10).

Skeletal muscles of Duchenne muscular dystrophy patients present Cx40.1, Cx43 and Cx45

Biopsy specimens from two patients with DMD and from one patient with Becker's muscular dystrophy (BMD), showing the absence and reduction of reactivity to dystrophin, respectively, and whose diagnosis were confirmed through the genetic analysis (Table 1). Assuming that the anti-Cx39 antibodies used cross react with Cx40.1, the Cx39 ortholog found in human [43], all human samples from dystrophic patients (2 DMD and 1 BMD) exhibited positive reactivity to Cx40.1, Cx43 and Cx45 that was not detected in two human control biopsies; one example of control and DMD is shown in Fig. 11.

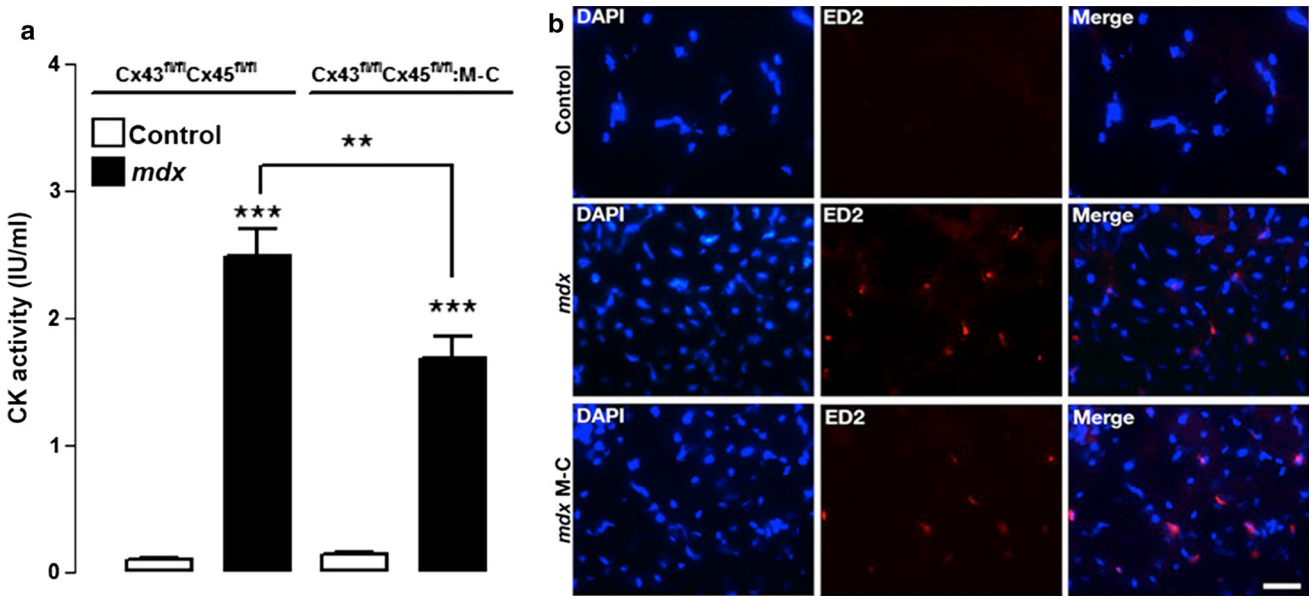

Fig. 9 The absence of Cx43/Cx45 expression reduces the activity of circulating creatine kinase activity but does not affect the infiltration of inflammatory cells. **a** *Graph* showing creatine kinase (CK) activity of control, *mdx* $Cx43^{fl/fl}$ $Cx45^{fl/fl}$ and *mdx* $Cx43^{fl/fl}$ $Cx45^{fl/fl}$:Myo-Cre (*mdx* M-C) mice. $n = 4$, $^{**}P < 0.01$, $^{***}P < 0.005$. **b** Panels showing TA muscles cross sections (20 µm thick) from (*top*) control (*middle*) *mdx* and (*bottom*) *mdx* $Cx43^{fl/fl}$ $Cx45^{fl/fl}$ (*mdx* M-C) mice with DAPI stained nuclei and infiltrated macrophages detected by their ED2 (*red*) reactivity. *Calibration bar* 50 µm

Discussion

The results of the present study indicate that skeletal muscles from patients diagnosed with DMD or BMD and *mdx* mice (animal model of DMD) express Cxs (39, 43 and 45). Accordingly, fast myofibers of *mdx* mice also express Cxs that form functional hemichannels co-expressed with other non-selective membrane channels. The presence of Cxs in myofibers was associated with activation of NF-κB, expression of iNOS and apoptotic cell death. The absence of Cx43/Cx45 expression in *mdx* myofibers abrogated all the above changes and partially reduced necrotic cell death and improved muscle performance. These findings suggest that Cx HCs play a critical role in muscle degeneration associated with muscular dystrophy.

In addition to *de novo* expression of Cxs 39, 43 and 45, *mdx* myofibers showed upregulation of Panx1 channels and de novo expression of two other non-selective membrane channels, $P2X_7R$ and TRPV2, as described previously [16, 17, 19]. Notably, the absence of Cx43/Cx45 expression by *mdx* fibers abrogated the expression of TRPV2 as observed by western blots and immunofluorescence assays, suggesting that TRPV2 expression is controlled downstream of Cx43/Cx45 expression. In contrast $P2X_7R$ and Cx39 expression in fibers of *mdx* $Cx43^{fl/fl}Cx45^{fl/fl}$:Myo-Cre mice was comparable to that of control *mdx* $Cx43^{fl/fl}Cx45^{fl/fl}$ fibers, suggesting that it is controlled independently or upstream of Cx43/Cx45 expression. The possible link between dystrophin and the expression of these non-selective membrane channels remains to be elucidated.

Clearly, all the non-selective channels mentioned above could contribute to the increase in sarcolemma permeability to Ca^{2+} in *mdx* myofibers, because they are all permeable to this divalent ion [15, 16, 19]. Consequently, each could partially contribute to reaching a critical intracellular free Ca^{2+} concentration that leads to cell degeneration. In support of this possibility, it has been shown that *mdx* myofibers express TRPV2 channels and $P2X_7R$, and that TRPV2 knockout or $P2X_7R$ inhibition reduces the intracellular Ca^{2+} signal [16, 19]. Moreover, we found that myofibers deficient in Cx43/Cx45 expression present similar free Ca^{2+} signal as control myofibers, whereas *mdx* myofibers presented a discrete by significant increase in basal free Ca^{2+} signal. These findings suggest that under basal condition, the Ca^{2+} handling mechanisms of *mdx* myofibers are slightly overfilled and the elimination of at least one Ca^{2+} permeable channel is enough to help the cells handle the Ca^{2+} influx mediated by the remaining Ca^{2+} permeable channels. These non-selective membrane channels could also increase Na^+ influx and high intracellular Na^+ concentration would interfere with Ca^{2+} extrusion via the Na^+/Ca^{2+} exchanger, thus reducing the Ca^{2+} handling capacity of myofibers as previously proposed [44]. In addition to the increase in permeability to Ca^{2+}, we found an increase in sarcolemma permeability to small molecules, including EB^{4-} (in vivo) and Etd^+

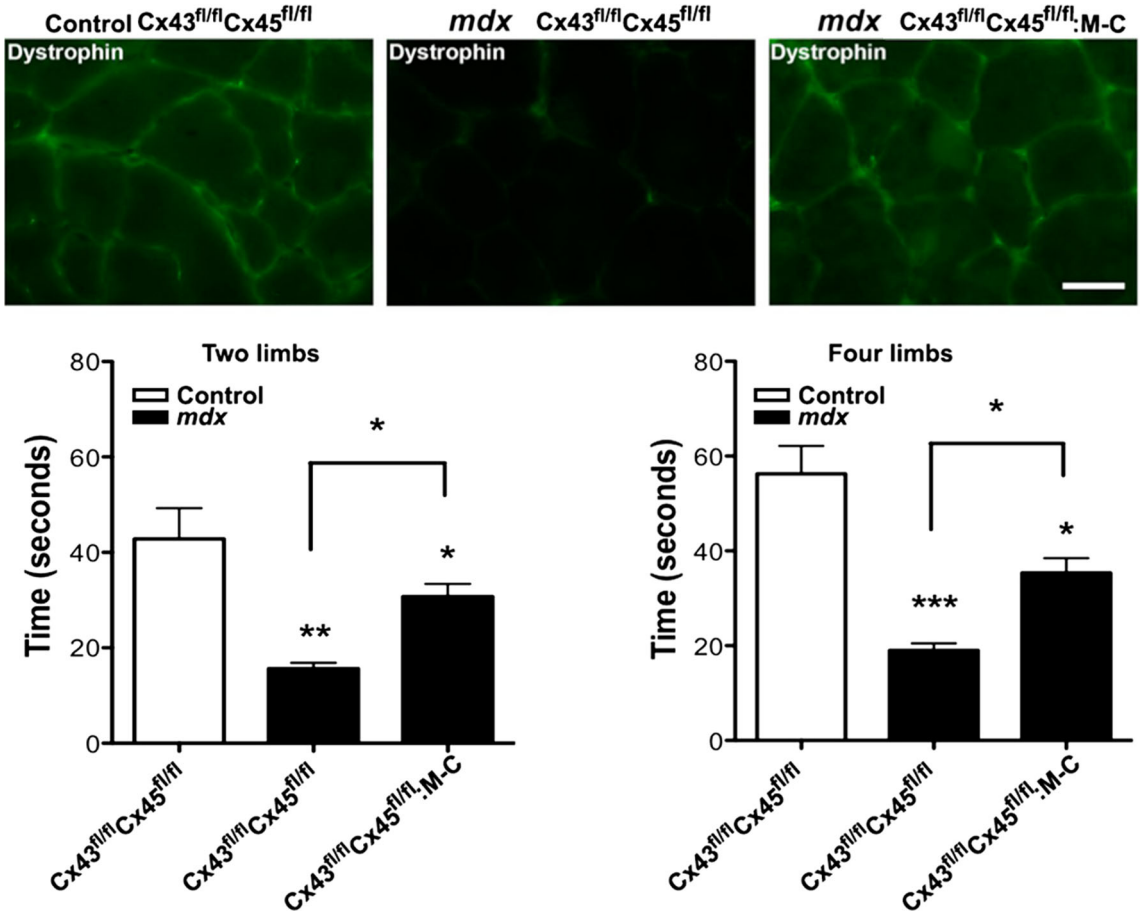

Fig. 10 The absence of Cx43/Cx45 upregulates the dystrophin immunoreactivity and improves muscle performance. The presence of dystrophin (*green*) was evaluated by immunofluorescence, in cross sections of control (C57) (*top left panel*) *tibialis anterior* muscle, *mdx* $Cx43^{fl/fl}Cx45^{fl/fl}$ (*top middle panel*) and *mdx* $Cx43^{fl/fl}Cx45^{fl/fl}$:Myo-Cre (*top right panel*) mice. *Scale bar* 50 μm (4 mice and 6 sections analyzed from each animal). Muscle performance was evaluated with the two (*bottom left graph*) and four (*bottom right graph*) leg hanging tests. $n = 4$, $^{*}P < 0.05$, $^{**}P < 0.01$, $^{***}P < 0.005$

(in vitro), which is reminiscent of what was described for denervated skeletal muscles [9]. These findings also indicate that cell staining with EB^{4-} results from dye influx via Cx HCs and not from cell membrane damage as interpreted elsewhere [45]. In agreement with this interpretation, EB^{4-} uptake of *mdx* myofibers was completely prevented by the acute administration of CBX or BBG, which are inhibitors of Cx HCs and Panx1 channels (CBX) and Panx1 channels and $P2X_7R$ [28]. This suggests that these channels play a critical role in *mdx* sarcolemma permeabilization to small molecules. In support of the role of Cx HCs, we have previously shown that Cx39 HCs, Cx43 HCs and Cx45 HCs are permeable to EB^{4-} [9]. In addition, we observed that myofibers of *mdx* mice were not stained in vivo with RD (molecular mass 10 kDa), which is a dye with a size well above the exclusion limit of any of the non-selective channels described herein. This finding also indicates that cells positive to extracellular proteins (e.g., Albumin, IgG and IgM; with molecular sizes well above the exclusion limit of Cx HCs) in DMD and *mdx* muscles [46] should be different from the EB^{4-}-stained cells and might be cells undergoing necrosis (see below).

The absence of Cx43/Cx45 in *mdx* myofibers was also sufficient to completely prevent Etd^{+} uptake of isolated *mdx* myofibers. In support of the role of non-selective channels, Etd^{+} uptake was completely inhibited by Cx HC (La^{3+}) or P2XR (oATP or A740003) blockers and partially blocked by the ^{10}Panx1 peptide, a Panx1 channel blocker. This point to the orchestration of these three channel types as it occurs in denervated myofibers [9]. Young et al. [19] observed the absence of propidium iodide uptake in *mdx* myoblasts and myotubes upon prolonged $P2X_7R$ activation. This finding might be explained by the low permeability of Cx HCs to propidium iodide [47]. However, the lack of Lucifer yellow uptake under these conditions [19] might be related to cellular differences since EB^{4-} is larger and more negatively charged (molecular mass 960.8 Da and −4 net charge) than Lucifer

Table 1 Data of patients with Duchenne or Becker muscular dystrophy included in this study

Patient	Gender/age of diagnosis (years)	Clinical features	Serum creatine kinase (U/l)	Skeletal muscles biopsy	Mutation in dystrophin gene	Diagnosis
DMD1105	M/2	Hypotonia Developmental delay	11,000–16,000	Large variability of myofiber size and increased centralization of nuclei Fatty infiltration and endomysial fibrosis Negative reactivity to dystrophin 1, 2 and 3	Frameshift deletion of exon 50	Duchenne's muscular dystrophy
DMD1073	M/3	Pseudohypertrophy of lower limbs Symmetrical hyporeflexia Gower (+)	4000–14,000	Large variability of myofiber size with frequent centered nuclei Intense necrosis-regeneration, fatty infiltration and endomysial fibrosis Negative reactivity to dystrophin 1, 2 and 3 Variable and weak reactivity to β-sarcoglycan	Point mutation c. 7585<T (GAA>TAA) Glu2529stop	Duchenne's muscular dystrophy
DMD1022	M/44	Muscular weakness of upper and lower limbs	1400	Large variability of myofiber size with frequent centered nuclei Scattered necrosis-regeneration with mild fatty infiltration Positive but irregular reactivity to dystrophin 1 and 3, and δ-sarcoglycan	In-frame deletion of exons 45–48	Becker's muscular dystrophy

yellow (MW: 443.4 and −2) and both dyes (EB^{4-} and LY^{2-}) have been shown to permeate Cx HCs [9, 48].

Dystrophic muscles show upregulation of NF-κB and iNOS activity and these responses can be ameliorated by reducing either the Ca^{2+} influx or Ca^{2+} release from intracellular stores [49]. Accordingly, we found that myofibers of *mdx* $Cx43^{fl/fl}Cx45^{fl/fl}$:Myo-Cre *mdx* mice, which are deficient in two Cx HCs, two membrane pathways for Ca^{2+} influx, present basal intracellular free Ca^{2+} signal comparable to that of control C57 myofibers, suggesting that the elevated basal Ca^{2+} signal found in *mdx* myofibers is the result of functional Cx HC expression. In addition, *mdx* $Cx43^{fl/fl}Cx45^{fl/fl}$:Myo-Cre *mdx* myofibers did not show NF-κB activation and iNOS expression. These findings suggest that selective inhibition of Cx HCs might be useful to reduce or completely inhibit the inflammasome activation and subsequent generation of proinflammatory cytokines as well as nitric oxide generation, which are elevated in *mdx* muscles [50, 51].

The observation of apoptosis in skeletal muscles of *mdx* mice was first reported by two groups [7, 34]. Consistent with our finding of colocalization of annexin V reactivity and EB^{4-} staining in fast myofibers of *mdx* mice, Matsuda and collaborators had shown that apoptotic myofibers are also stained with EB^{4-} [7]. We now demonstrated that myofibers deficient in Cx43/Cx45 do not exhibit evident apoptosis, which again is consistent with the combined action of different non-selective membrane channels. In line with the latter, the dominant negative inhibition of TRPV2 channels drastically reduced apoptosis and EB^{4-} stained myofibers of *mdx* mice [16]. Since TRPV2 channels are impermeable to EB^{4-} [9] and Cx HC activity is promoted by elevated intracellular Ca^{2+} concentrations [10], the reduction in EB^{4-} staining described by Iwata and collaborators [16] might be explained by the resulting reduction in intracellular Ca^{2+} concentration that would prevent activation of Cx HCs [10].

Mdx mice also exhibit myofiber necrosis, which as a result of the cell lysis induces macrophage infiltration and elevates serum levels of cytosolic proteins including CK [16, 34]. Here, we found that the absence of Cx43/Cx45 expression does not significantly affect the muscle infiltration of ED2 positive cells and only partially prevented (∼30 %) the increase in serum CK levels of *mdx* mice. Similarly, *mdx* mice under dominant negative inhibition of TRPV2 channels have been shown to present lower serum CK levels than untreated *mdx* mice [16]. Inhibition of TRPV2 channels should result in systemic inhibition whereas Cx43/Cx45 KO was restricted to myofibers. It should be noted that necrosis is frequently triggered by ischemia–reperfusion or hypoxia–reoxygenation, and the absence of dystrophin in other cell types might contribute to these processes affecting myofiber survival. In fact, dystrophin is expressed in platelets [45] and tunica media

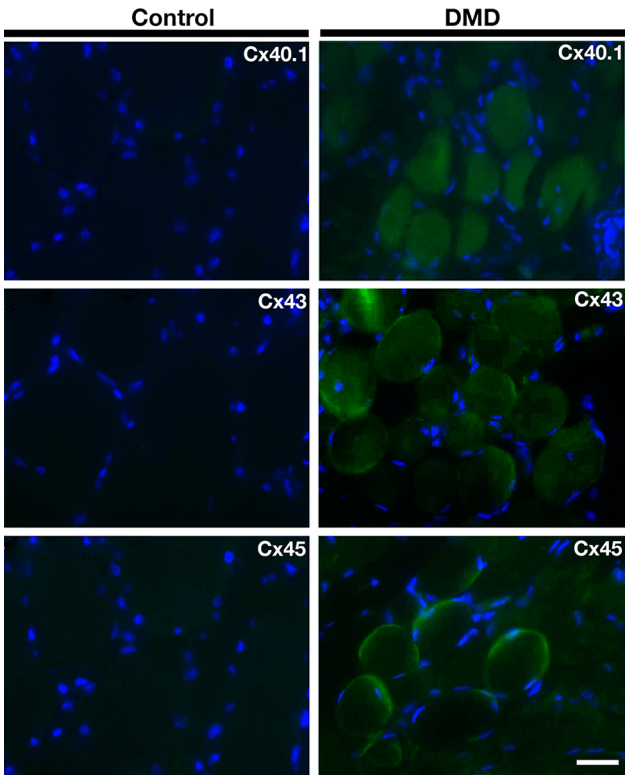

Fig. 11 Connexins 40.1, 43 and 45 are present in human biopsies of Duchenne muscular dystrophy patients but not of normal subjects. Sections of biopsies from quadriceps muscles were obtained from a Spanish Duchenne muscular dystrophy patient (DMD, *right panels*) and control person (control, *left panels*). The presence of connexins 40.1, 43 or 45 (Cx40.1, Cx43 and Cx45) was analyzed by immunofluorescence assays in three muscle sections. *Scale bar* 50 μm (2 DMD patients)

of blood vessels [52], and its absence in blood vessel of patients with DMD has been reported [52]. Consequently, dystrophin deficiency in these cells might explain the multiple episodes of thrombosis found in patients with BMD, which is a less aggressive muscle dystrophy than DMD [53]. Treatment with a vasodilator could, thus, alleviate muscle ischemia in patients with BMD [54]. In support of the orchestration of several non-selective channels treatment with Coomassie brilliant blue, which is a blocker of $P2X_7Rs$, reduces the number of degeneration–regeneration cycles in *mdx* mice [19].

Regeneration, internal nuclei, hypertrophic cells are other common changes found in muscles of *mdx* mice or DMD patients [46]. Similarly, we found numerous intracellularly nucleated and hypertrophic myofibers in TA muscles of *mdx* mice. However, both changes were significantly reduced in muscles of mice deficient in Cx43/Cx45 expression, thus suggesting that necrosis was reduced but not completely eliminated.

Muscles of *mdx* mice deficient in Cx43/Cx45 remarkably showed dystrophin expression comparable to that of control C57BL/6 mice. This might result from less Ca^{2+} influx via Cx HCs and TRPV2 channels, hence reducing the activation of Ca^{2+}-dependent proteases and reducing proteolysis of numerous proteins, including dystrophin. Despite the presence of high levels of dystrophin in Cx43/Cx45 deficient muscles the muscle function evaluated in the whole animals showed only partial protection compared to control mice. This is probably because the rescued dystrophin is not functional or is just partially functional. It remains to be determined whether selective inhibition of Cx HC in other tissue including the heart, vascular cells and platelets would confer more significant protection in all parameters described here as partially protected. Alternatively, the simultaneous inhibition of all non-selective channels mentioned here might be more effective in protecting *mdx* mice.

Because we detected the presence of Cxs in skeletal muscle from patients diagnosed with DMD and BMD, based on the observation that these proteins form functional hemichannels and that the absence of Cx43/Cx45 prevented the apoptosis in *mdx* myofibers, we suggest that these channels could constitute a potential therapeutic target to reduce muscle deterioration in DMD or BMD.

Materials and methods

Reagents

Western lightning chemiluminescence (ECL) detection reagents were obtained from PerkinElmer (Boston, MA, USA) was purchased from Pierce (Pierce biotechnology, Rockford, IL, USA), and anti-rabbit or anti-mouse IgG antibodies-conjugated to Cy2 (green) or Cy3 (red) were purchased from Jackson immunoresearch laboratories (West Grove, PA, USA). Ethidium (Etd^+) bromide was from GIBCO/BRL (*Grand Island*, NY, USA), fluoromount-G was from Electron Microscopy Science (Hatfield, PA, USA), brilliant blue G (BBG), *N*-benzyl-*p*-toluene sulphonamide (BTS) and collagenase type I were obtained from Sigma (St. Louis, USA), and A740003 from Tocris Bioscience (Bristol, UK). Phycoerithrin (PE) or FITC conjugated monoclonal anti-annexin V antibody were from BD Biosciences (San Jose, CA, USA) and polyclonal anti-TRPV2 or anti-$P2X_7R$ antibodies were from Abcam (Cambridge, MA, USA). Previously described polyclonal anti-Cx39, -43, -Cx45, and -Panx1 antibodies were used [9]. Rabbit polyclonal anti-phosphorylated-p65 NF-kB subunit antibodies were from Cell Signaling, and rabbit polyclonal anti-dystrophin antibodies were from the Developmental Studies Hybridoma Bank.

The dystrophin monoclonal antibody (MANDRA1) developed by Glenn E. Morris was obtained from the

Developmental Studies Hybridoma Bank developed under the auspices of the NICHD and maintained by The University of Iowa, Department of Biology, Iowa City, IA 52242, USA.

Animals

All protocols were approved by the Bioethics Committee of the Pontificia Universidad Católica de Chile (protocol no. 176) in accordance with the ethical standards laid down in the 1964 Declaration of Helsinki and its later amendments. All efforts were made to minimize animal suffering, reduce the number of animals used, and alternatives to in vivo techniques, if available. Two- to three-month-old male C57BL/6 (C57) and *mdx* mice (C57BL/6 *mdx*^{4cv}) were obtained from the animal facility of the Faculty of Biological Sciences at the Pontificia Universidad Católica de Chile. Previously described Cx43$^{fl/fl}$Cx45$^{fl/fl}$ and Cx43$^{fl/fl}$Cx45$^{fl/fl}$:Myo-Cre mice were used [9]. The latter were skeletal muscle deficient for Cx43 and Cx45 generated from breeding Cx43$^{fl/fl}$ mice [55] and Cx45$^{fl/fl}$ mice [56] with Myo-Cre mice, which express Cre recombinase under the control of a myogenin promoter and the MEF2C [57] enhancer. *Mdx* mice lacking Cx43 and Cx45 expression in skeletal muscle were obtained by a four-factor cross starting with mating a Cx43- and Cx45-deficient (in skeletal muscle) male mouse to a homozygous mdx female (the mdx mutation is located on the X chromosome). This led to offspring, all being heterozygously floxed for Cx43 and Cx45, of which 50 % showed Myo-Cre expression but all carried the mutated X chromosome (F1 generation). For generating the F2 generation a Cx43$^{fl/+}$ Cx45$^{fl/+}$, mdx/x female was bred with a Cx43$^{fl/fl}$ Cx45$^{fl/fl}$:Myo-Cre male to generate the desired genotype Cx43$^{fl/fl}$ Cx45$^{fl/fl}$:Myo-Cre, mdx/y male. Breeding this male (F2) with Cx43$^{fl/fl}$ Cx45$^{fl/fl}$, mdx/+ females finally yielded the desired mutants in the F3 generation Cx43$^{fl/fl}$ Cx45$^{fl/fl}$:Myo-Cre, mdx/mdx females and Cx43$^{fl/fl}$ Cx45$^{fl/fl}$:Myo-Cre, mdx/y males which were interbred.

Genotyping of *mdx* mice

Genomic DNA from a tail piece (2 mm) was isolated using the proteinase K digestion method [58] and http://jackslab.mit.edu/protocols/dna_isolation_proteinase_k_method, with some modifications. Briefly, samples were incubated overnight in 400 µl of lysis buffer (0.5 % SDS, 100 mM NaCl, 10 mM EDTA and 10 mM Tris–HCl pH 8) containing 300 µg of proteinase K at 55 °C. Then, 300 µl of 6 M NaCl were added, mixed and samples were spun down at 13,000*g* for 10 min at room temperature (RT). The supernatant was transferred to a new microcentrifuge tube and 700 µl of isopropanol were added, mixed and incubated at RT for 15 min. Samples were spun down at 13,000*g* for 10 min at RT. Finally, DNA pellet was rinse with 70 % ethanol, air dried and resuspended in 50 µl of nuclease-free water. An aliquot of genomic DNA was diluted 1:10 and 1 µl was used for PCR. Genotyping was performed by primer competition PCR method described previously [59]. This method allows identifying the *mdx* and wild type genotype mice by different sizes of PCR products. A product of 123 pb confirms the *mdx*^{4cv} genotype and for WT genotype the PCR product is 141 pb.

Western blots

Tibialis anterior muscles were washed with ice-cold saline. Tendon-free muscles were minced in small pieces by using a razor blade and then homogenized (homogenizer; Brinkmann) and sonicated (Heat Systems Microson). Tissue homogenates were centrifuged for 15 min at 13,000×*g* and pellets were discarded. Then, samples were processed for western blot analyses of proteins of interest as described previously [25]. Blots were incubated overnight with appropriate dilutions of primary antibodies diluted in 5 % fat free milk–PBS solution. Then, blots were rinsed with 1 % PBS solution–Tween 20 and incubated for 40 min at room temperature with HRP-conjugated goat anti-rabbit or anti-mouse IgGs (Santa Cruz Biotechnology). After five rinses, immunoreactive proteins were detected using ECL reagents according to the manufacturer's instructions (PerkinElmer).

Skeletal myofibers isolation

Myofibers of mouse flexor digitorum brevis (FDB) muscles were isolated from anesthetized mice as described previously [9]. Muscles were immersed in cultured medium (DMEM/F12 supplemented with 10 % fetal bovine serum) containing 0.2% collagenase type I and incubated for 2.5 h at 37 °C. Then, they were transferred to a 15 ml Falcon test tube containing 3 ml of Krebs buffer (in mM: 145 NaCl, 5 KCl, 3 $CaCl_2$, 1 $MgCl_2$, 5.6 glucose, 10 HEPES-Na, pH 7.4) plus 10 µM BTS (to reduce muscle damage due to activation of myofiber contraction during the isolation procedure). Muscle tissue was incubated for 5 min with 200 µM Suramin, which is a P2 receptor inhibitor, to prevent activation of P2 receptors by ATP released during the isolation procedure. Then, tissue was gently triturated by passing it 15 times through a wide-tip Pasteur pipette so as to dissociate single myofibers. Dissociated myofibers were centrifuged at 1000 rpm for 10 s (Kubota 8700 centrifuge, Tokyo, Japan) and the sediment was washed two times with HEPES buffered Krebs saline solution containing 10 µM BTS. Finally, myofibers were resuspended in 5 ml HEPES buffered Krebs solution plus 10 µM BTS,

plated in plastic culture dishes or placed in 1.5 ml Eppendorf tubes.

Membrane permeability to dyes

The uptake of fluorescent molecules was evaluated using time lapse measurements or snap shot photographs. Freshly isolated myofibers plated onto plastic culture dishes were washed twice with Krebs-buffer solution. For time lapse measurements myofibers were incubated in Krebs buffer solution (plus 10 μM BTS) containing 5 μM ethidium (Etd^+) bromide. Etd^+ fluorescence was recorded in regions of interest located in nuclei of the myofibers. A water immersion Olympus 51W1I upright microscope (Japan) was used for recording. Images were captured with a Q Imaging model Retiga 13001 fast cooled monochromatic digital camera (12-bit) (Qimaging, Burnaby, BC, Canada) every 30 s. Image processing was performed off-line with ImageJ software (NIH, Bethesda, USA).

For snap shot pictures frozen sections of *tibialis anterior* (TA) muscles from mice injected with EB^{4-} were analyzed by epifluorescence microscopy (excitation 495 nm, emission 590 nm).

Ca^{2+} signal measurements

The basal intracellular free Ca^{2+} signal was measured in isolated myofibers using the Ca^{2+} indicator FURA-2AM and following the manufacturer's instructions. Briefly, isolated myofibers were incubated with FURA-2AM (5 μM) in Krebs solution for 50 min at room temperature. Once finished the incubation period, the myofibers were washed with Krebs saline solution without dye, and placed on coverslips to measure the basal free Ca^{2+} signal in fluorescence microscope Nikon eclipse *Ti* (Tokyo, Japan) as the 340 nm:380 nm fluorescence ratio.

Immunofluorescence analysis

To detect different proteins in myofibers or cross sections (20 μm) of muscles (fast frozen with iso-methyl-butane cooled in liquid nitrogen) samples were obtained and processed as described previously [9]. Samples were incubated at 4 °C for 12 h with diluted primary anti-Cx39 (1:100), anti-Cx43 (1:300), anti-Cx45 (1:300), anti-Panx1 (1:300), anti-TRPV2 (1:100), anti-$P2X_7$ (1:300) or anti-phosphorylated P65 (1:200) antibodies followed by four washes with HSS and then, incubated with an appropriate dilution of Cy2- or Cy3-conjugated goat anti-rabbit IgG antibodies. Samples were rinsed with HSS, mounted with fluoromount G on glass slides and representative images were acquired in a confocal microscope, Olympus fluoview 1000 (Tokyo, Japan).

For annexin and active caspase 3 detection cross sections of tibialis anterior (TA) muscle were mounted on slides, fixed for 5 min with formaldehyde 4 % w/v and then incubated with blocking solution (NH_4Cl 50 mM, BSA 1 %, PBS1X) for 3 h at room temperature. Then, the slices were incubated for 12 h at 4 °C with anti-annexin V antibody conjugated to phycoerythrin or anti-active caspase 3 antibody followed by incubation with a secondary antibody conjugated to FIT-C and washed three times with PBS. Samples were subsequently covered with fluoromount G and glass coverslips. The slices were analyzed with a fluorescence microscope Nikon Eclipse *Ti*.

The absence of dystrophin in *mdx* mice was confirmed by immunological detection with anti-dystrophin antibodies.

Cross-sectional area (CSA) and centered nuclei

The CSA of skeletal muscle fibers was measured as described previously [9]. In brief, cryosections of muscles were fixed with 4 % (wt/vol) paraformaldehyde, stained with hematoxylin and eosin and mounted with fluoromount G with DAPI on glass slide for nuclei detection. The CSA of each myofiber was evaluated by using offline analyses with ImageJ software (National Institutes of Health).

Internal nuclei index

Skeletal muscle sections with hematoxylin/eosin and DAPI stained were used. In brief, the internal nucleus in each myofiber and total myofibers in each image were counted. The index was calculated as the ratio between the total internal nuclei and total myofibers in each image.

Creatine kinase activity

Blood was obtained from adult mice (8–9 weeks, ~20 g). The collected blood was incubated (45–60 min) at 37 °C to allow blood to clot. Then, samples were centrifuged (1000 rpm for 5 m) to remove the clot, and the clear supernatant was the serum. The catalytic activity of serum creation kinase was determined at 37 °C on a spectrophotometer at 340 nm in accordance with manufacture's instructions (Valtek S.A., Santiago, Chile).

Wire hanging test

A metal cloth hanger was hanged around 37 cm above a layer of bedding. Then, a mouse was brought near the wire via the tail. For two limb hanging test, the mouse was left to grasp the wire with two forepaws only, and the hind limbs were lowered in such a way that the mouse only hanged by the two forepaws from the wire. The maximum

hanging time was recorded. For four limb hanging test, the mouse was led to grasp in the wire with four limbs, for which the maximum hanging time was recorded.

Selection of DMD patients and mutation and biopsy studies

Following ethical guidelines, the healthy volunteers and DMD patients who participated in this study signed an informed consent approved by the local Ethics Committee in accordance with the ethical standards laid down in the 1964 Declaration of Helsinki and its later amendments. Diagnosis of Duchenne/Becker muscular dystrophy was achieved based on clinical examination, muscular biopsy and mutation analysis (Table 1). Genomic DNA extracted from peripheral blood leucocytes by standardized procedures (kit Purogene, Qiagen GmbH, Hilden, Germany) were screened for DMD gene duplications/deletions using the MLPA technique (SALSA MLPA probemixes P034/P035 DMD, MRC-Holland, Amsterdam, The Netherlands). In those cases without duplications/deletions, the 79 exons of the *DMD* gene and part of the intronic regions were sequenced by NGS technology by the Illumina MiSeq team. The amplified fragments were performed using the Multiplicom MASTR DMD kit. All variants detected were confirmed by Sanger sequencing (amplified DNA products were sequenced by the dideoxy termination method, BigDye Sequencing Kit, Applied Biosystems, Foster City, CA, USA). Human biopsies from controls and DMD patients consisted of small fragments of quadriceps muscle and were quickly frozen with isopentane in a container immersed in liquid nitrogen. Cryosections of 10 μm fixed in 4 % paraformaldehyde were processed for histological (H–E and trichrome), histochemical stains [oxidative (NADH, SDH and COX), ATPasa (pH 4.2; 4.6 and 9.4), Oil-red-O and PAS] and immunohistochemistry (dystrophin 1, 2 and 3, alpha, beta, delta and gamma sarcoglycans, merosin and beta-spectrin and Cxs).

Statistical analysis

Results are presented as mean ± standard error (SE). Two populations were compared using the logarithm of ratio and posterior Student's *t* test. For multiple comparisons with a single control, a non-parametric one-way ANOVA followed by the Tukey's multiple comparison test was used. Analyses were carried out using GRAPHPAD software. $P < 0.05$ was considered statistically significant.

Acknowledgments We thank Ms. Teresa Vergara and Ms. Paola Fernández for their technical support. We also thank members of the Spanish families, whose participation made this study possible. This work was partially supported by CONICYT/PAI Proyecto de Inserción en la Academia 79140023 (to LAC); Fondo Nacional de Desarrollo Científico y Tecnológico (FONDECYT): Grant 3130662 (to CP); 1150291 (to JCS), ICM-Economía P09-022-F Centro Interdisciplinario de Neurociencias de Valparaíso (to JCS), grants from the Spanish Ministry of Economy and Competitiveness (Consolider CSD2008-00005 and BFU2013-33821) and the Community of Madrid (Neurotec-P2010/BMD-2460*)* (to LCB). The research stay of LAC and CP in the Bonn laboratory was supported by a grant of CONICYT and the German Academic Exchange Service (to JCS and KW). Additional work in the Bonn laboratory was funded by the German Research Foundation (Wi 270/33.1 and SFB 645, B2) to KW.

Compliance with ethical standards

Conflict of interest The authors declare that they have no conflict of interest.

Ethical standards The authors certify that the experiments comply with the current laws of Chile, where the experiments were performed. All protocols were approved by the Bioethics Committee of the Pontificia Universidad Católica de Chile (Protocol No. 176) in accordance with the ethical standards laid down in the 1964 Declaration of Helsinki and its later amendments. All efforts were made to minimize animal suffering, reduce the number of animals used, and alternatives to in vivo techniques, if available.

References

1. Emery AE (2002) Muscular dystrophy into the new millennium. Neuromuscul Disord 12:343–349
2. Ervasti JM, Campbell KP (1993) A role for the dystrophin–glycoprotein complex as a transmembrane linker between laminin and actin. J Cell Biol 122:809–823
3. Pillers D (2014) A new day for Duchenne's? The time has come for newborn screening. Mol Genet Metab 113:11–13
4. Bulfield G, Siller WG, Wight PA, Moore KJ (1984) X chromosome-linked muscular dystrophy (mdx) in the mouse. Proc Natl Acad Sci USA 81:1189–1192
5. Balnave CD, Allen DG (1995) Intracellular calcium and force in single mouse muscle fibres following repeated contractions with stretch. J Physiol 488:25–36
6. Yeung EW, Head SI, Allen DG (2003) Gadolinium reduces short-term stretch-induced muscle damage in isolated mdx mouse muscle fibres. J Physiol 552:449–458
7. Matsuda R, Nishikawa A, Tanaka H (1995) Visualization of dystrophic muscle fibers in mdx mouse by vital staining with Evans blue: evidence of apoptosis in dystrophin-deficient muscle. J Biochem 118:959–964
8. Hamer PW, McGeachie JM, Davies MJ, Grounds MD (2002) Evans Blue Dye as an in vivo marker of myofibre damage: optimising parameters for detecting initial myofibre membrane permeability. J Anat 200:69–79
9. Cea LA, Cisterna BA, Puebla C, Frank M, Figueroa XF, Cardozo C et al (2013) De novo expression of connexin hemichannels in denervated fast skeletal muscles leads to atrophy. Proc Natl Acad Sci USA 110:16229–16234
10. Sáez JC, Leybaert L (2014) Hunting for connexin hemichannels. FEBS Lett 588:1205–1211
11. Eskandari S, Zampighi GA, Leung DW, Wright EM, Loo DD (2002) Inhibition of gap junction hemichannels by chloride channel blockers. J Membr Biol 185:93–102
12. Franco A Jr, Lansman JB (1990) Calcium entry through stretch-inactivated ion channels in mdx myotubes. Nature 344:670–673
13. Bao L, Sachs F, Dahl G (2004) Connexins are mechanosensitive. Am J Physiol Cell Physiol 287:C1389–C1395

14. Fiori MC, Figueroa V, Zoghbi ME, Saéz JC, Reuss L, Altenberg GA (2012) Permeation of calcium through purified connexin 26 hemichannels. J Biol Chem 287:40826–40834
15. Schalper KA, Sánchez HA, Lee SC, Altenberg GA, Nathanson MH, Sáez JC (2010) Connexin 43 hemichannels mediate the Ca^{2+} influx induced by extracellular alkalinization. Am J Physiol Cell Physiol 299:C1504–C1515
16. Iwata Y, Katanosaka Y, Arai Y, Shigekawa M, Wakabayashi S (2009) Dominant-negative inhibition of Ca^{2+} influx via TRPV2 ameliorates muscular dystrophy in animal models. Hum Mol Genet 18:824–834
17. Valladares D, Almarza G, Contreras A, Pavez M, Buvinic S, Jaimovich E et al (2013) Electrical stimuli are anti-apoptotic in skeletal muscle via extracellular ATP. Alteration of this signal in mdx mice is a likely cause of dystrophy. PLoS One 8:e75340
18. Yeung D, Zablocki K, Lien CF, Jiang T, Arkle S, Brutkowski W et al (2006) Increased susceptibility to ATP via alteration of P2X receptor function in dystrophic mdx mouse muscle cells. FASEB J 20:610–620
19. Young CN, Brutkowski W, Lien CF, Arkle S, Lochmüller H, Zabłocki K et al (2012) $P2X_7$ purinoceptor alterations in dystrophic mdx mouse muscles: relationship to pathology and potential target for treatment. J Cell Mol Med 16:1026–1037
20. Kondo RP, Wang SY, John SA, Weiss JN, Goldhaber JI (2000) Metabolic inhibition activates a non-selective current through connexin hemichannels in isolated ventricular myocytes. J Mol Cell Cardiol 32:1859–1872
21. Sáez JC, Schalper KA, Retamal MA, Orellana JA, Shoji KF, Bennett MV (2010) Cell membrane permeabilization via connexin hemichannels in living and dying cells. Exp Cell Res 316:2377–2389
22. North RA (2002) Molecular physiology of P2X receptors. Physiol Rev 82:1013–1067
23. Perálvarez-Marín A, Doñate-Macian P, Gaudet R (2013) What do we know about the transient receptor potential vanilloid 2 (TRPV2) ion channel? FEBS J 280:5471–5487
24. Cea LA, Riquelme MA, Cisterna BA, Puebla C, Vega JL, Rovegno M et al (2012) Connexin- and pannexin-based channels in normal skeletal muscles and their possible role in muscle atrophy. J Membr Biol 245:423–436
25. Riquelme MA, Cea LA, Vega JL, Boric MP, Monyer H, Bennett MV et al (2013) The ATP required for potentiation of skeletal muscle contraction is released via pannexin hemichannels. Neuropharmacology 75:594–603
26. Riquelme MA, Cea LA, Vega JL, Puebla C, Vargas AA, Shoji KF et al (2015) Pannexin channels mediate the acquisition of myogenic commitment in C2C12 reserve cells promoted by P2 receptor activation. Front Cell Dev Biol 3:25 **(eCollection)**
27. Araya R, Eckardt D, Maxeiner S, Krüger O, Theis M, Willecke K, Sáez JC (2005) Expression of connexins during differentiation and regeneration of skeletal muscle: functional relevance of connexin43. J Cell Sci 118:27–37
28. Dahl G, Qiu F, Wang J (2013) The bizarre pharmacology of the ATP release channel pannexin1. Neuropharmacology 75:583–593
29. Nakazawa K, Liu M, Inoue K, Ohno Y (1997) Potent inhibition by trivalent cations of ATP-gated channels. Eur J Pharmacol 325:237–243
30. Honore P, Donnelly-Roberts D, Namovic MT, Hsieh G, Zhu CZ, Mikusa JP et al (2006) A-740003 [*N*-(1-{[(cyanoimino)(5-quinolinylamino) methyl]amino}-2,2-dimethylpropyl)-2-(3,4-dimethoxy phenyl)acetamide], a novel and selective P2X7 receptor antagonist, dose-dependently reduces neuropathic pain in the rat. J Pharmacol Exp Ther 319:1376–1385
31. Burr AR, Molkentin JD (2015) Genetic evidence in the mouse solidifies the calcium hypothesis of myofiber death in muscular dystrophy. Cell Death Differ 22:1402–1412
32. Bia BL, Cassidy PJ, Young ME, Rafael JA, Leighton B, Davies KE et al (1999) Decreased myocardial nNOS, increased iNOS and abnormal ECGs in mouse models of Duchenne muscular dystrophy. J Mol Cell Cardiol 31:1857–1862
33. Vannucchi MG, Corsani L, Azzena GB, Faussone-Pellegrini MS, Mancinelli R (2004) Functional activity and expression of inducible nitric oxide synthase (iNOS) in muscle of the isolated distal colon of mdx mice. Muscle Nerve 29:795–803
34. Tidball JG, Albrecht DE, Lokensgard BE, Spencer MJ (1995) Apoptosis precedes necrosis of dystrophin-deficient muscle. J Cell Sci 108:2197–2204
35. Turpin SM, Lancaster GI, Darby I, Febbraio MA, Watt MJ (2006) Apoptosis in skeletal muscle myotubes is induced by ceramides and is positively related to insulin resistance. Am J Physiol Endocrinol Metab 291:E1341–E1350
36. Percy ME, Andrews DF, Thompson MW (1982) Serum creatine kinase in the detection of Duchenne muscular dystrophy carriers: effects of season and multiple testing. Muscle Nerve 5:58–64
37. Glesby MJ, Rosenmann E, Nylen EG, Wrogemann K (1988) Serum CK, calcium, magnesium, and oxidative phosphorylation in mdx mouse muscular dystrophy. Muscle Nerve 11:852–856
38. Manning J, O'Malley D (2015) What has the mdx mouse model of duchenne muscular dystrophy contributed to our understanding of this disease? J Muscle Res Cell Motil 36:155–167
39. Lagrota-Candido J, Vasconcellos R, Cavalcanti M, Bozza M, Savino W, Quirico-Santos T (2002) Resolution of skeletal muscle inflammation in mdx dystrophic mouse is accompanied by increased immunoglobulin and interferon-gamma production. Int J Exp Pathol 83:121–132
40. Polfliet MM, Fabriek BO, Daniëls WP, Dijkstra CD, van den Berg TK (2006) The rat macrophage scavenger receptor CD163: expression, regulation and role in inflammatory mediator production. Immunobiology 211:419–425
41. Pigozzo SR, Da Re L, Romualdi C, Mazzara PG, Galletta E, Fletcher S et al (2013) Revertant fibers in the mdx murine model of Duchenne muscular dystrophy: an age- and muscle-related reappraisal. PLoS One 8:e72147
42. Hoffman EP, Brown RH Jr, Kunkel LM (1987) Dystrophin: the protein product of the Duchenne muscular dystrophy locus. Cell 51:919–928
43. von Maltzahn J, Euwens C, Willecke K, Söhl G (2004) The novel mouse connexin39 gene is expressed in developing striated muscle. J Cell Sci 117:5381–5392
44. Iwata Y, Katanosaka Y, Hisamitsu T, Wakabayashi S (2007) Enhanced Na^+/H^+ exchange activity contributes to the pathogenesis of muscular dystrophy via involvement of P2 receptors. Am J Pathol 171:1576–1587
45. Cerecedo D, Mondragón R, Cisneros B, Martínez-Pérez F, Martínez-Rojas D, Rendón A (2006) Role of dystrophins and utrophins in platelet adhesion process. Br J Haematol 134:83–91
46. Blake DJ, Weir A, Newey SE, Davies KE (2002) Function and genetics of dystrophin and dystrophin-related proteins in muscle. Physiol Rev 82:291–329
47. Orellana JA, Díaz E, Schalper KA, Vargas AA, Bennett MV, Sáez JC (2011) Cation permeation through connexin 43 hemichannels is cooperative, competitive and saturable with parameters depending on the permeant species. Biochem Biophys Res Commun 409:603–609
48. Garré JM, Retamal MA, Cassina P, Barbeito L, Bukauskas FF, Sáez JC et al (2010) FGF-1 induces ATP release from spinal astrocytes in culture and opens pannexin and connexin hemichannels. Proc Natl Acad Sci USA 107:22659–22664

49. Altamirano F, López JR, Henríquez C, Molinski T, Allen PD, Jaimovich E (2012) Increased resting intracellular calcium modulates NF-κB-dependent inducible nitric-oxide synthase gene expression in dystrophic mdx skeletal myotubes. J Biol Chem 287:20876–20887
50. Whitehead NP, Pham C, Gervasio OL, Allen DG (2008) *N*-Acetylcysteine ameliorates skeletal muscle pathophysiology in mdx mice. J Physiol 586:2003–2014
51. Lawler JM (2011) Exacerbation of pathology by oxidative stress in respiratory and locomotor muscles with Duchenne muscular dystrophy. J Physiol 589:2161–2170
52. Miyatake M, Miike T, Zhao J, Yoshioka K, Uchino M, Usuku G (1989) Possible systemic smooth muscle layer dysfunction due to a deficiency of dystrophin in Duchenne muscular dystrophy. J Neurol Sci 93:11–17
53. Higuchi I, Niiyama T, Uchida Y, Inose M, Nakagawa M, Arimura K et al (1999) Multiple episodes of thrombosis in a patient with Becker muscular dystrophy with marked expression of utrophin on the muscle cell membrane. Acta Neuropathol 98:313–316
54. Martin EA, Barresi R, Byrne BJ, Tsimerinov EI, Scott BL, Walker AE et al (2012) Tadalafil alleviates muscle ischemia in patients with Becker muscular dystrophy. Sci Transl Med 4:162ra155
55. Theis M, de Wit C, Schlaeger TM, Eckardt D, Krüger O, Döring B et al (2001) Endothelium-specific replacement of the connexin43 coding region by a lacZ reporter gene. Genesis 29:1–13
56. Maxeiner S, Dedek K, Janssen-Bienhold U, Ammermüller J, Brune H, Kirsch T et al (2005) Deletion of connexin45 in mouse retinal neurons disrupts the rod/cone signaling pathway between AII amacrine and ON cone bipolar cells and leads to impaired visual transmission. J Neurosci 25:566–576
57. Li S, Czubryt MP, McAnally J, Bassel-Duby R, Richardson JA, Wiebel FF et al (2005) Requirement for serum response factor for skeletal muscle growth and maturation revealed by tissue-specificgene deletion in mice. Proc Natl Acad Sci USA 102:1082–1087
58. Trebbin AL, Hoey AJ (2009) A novel and simple method for genotyping the mdx mouse using high-resolution melt polymerase chain reaction. Muscle Nerve 39:603–608
59. Shin JH, Hakim CH, Zhang K, Duan D (2011) Genotyping mdx, mdx3cv, and mdx4cv mice by primer competition polymerase chain reaction. Muscle Nerve 43:283–286